water

MDPI

Article

Modelling a Sediment Excluder in Irrigation Canals: A Case Study of the Koya Tami Irrigation Area, Jayapura

Herryan Kendra Kaharudin [1,*], Agustinus Purna Irawan [2] and Wati Asriningsih Pranoto [1]

[1] Doctoral Program in Civil Engineering, Faculty of Engineering, Universitas Tarumanagara, Jakarta 11440, Indonesia; watip@ft.untar.ac.id
[2] School of STEM, Universitas Prasetiya Mulya, Jakarta 12430, Indonesia; agustinus.irawan@prasetiyamulya.ac.id
* Correspondence: herryan.328232005@stu.untar.ac.id

Abstract

The Indonesian Irrigation Design Criteria (KP-02 and KP-04) provide limited guidance for cohesive sediment at irrigation intakes. This study investigates a modified four-channel silt settler using field observations from Warujayeng and Koya Tami Irrigation Area, Jayapura. The assessment combines sediment analyses, HEC-RAS 2D modelling, FLOW-3D Hydro simulations of two alternatives at settling and flushing discharges of 5.0 and 7.5 m^3/s, respectively, and hydraulic tests using a 1:5 physical model. Warujayeng downstream samples contained 74.59–75.01% silt and 20.97–21.79% clay, while cohesive fractions at Koya Tami reached 77–100%. Without baffles, settling opportunity indices were 0.48% for Alternative 2A and 0.02% for Alternative 2B, with surface loading rates of 2.19–8.14 m/h. Inlet baffles reduced the coefficient of variation in simulated channel-load distribution from 1.474 to 0.297–0.331. The projected settling opportunity index of 56.4–58.0% is an exploratory upper-bound estimate, not validated trapping efficiency. Full-gate-opening flushing removed 248.4 t and used 6.3% less water per kilogram of sediment removed than one-gate opening. Hydraulic validation yielded relative mean absolute errors of 6.43% for water level and 12.50% for velocity. Further cohesive-sediment transport tests are required to validate trapping performance.

Keywords: cohesive sediment; sediment excluder; silt settler; irrigation intake; sediment settling; inlet baffles; FLOW-3D Hydro; hydraulic physical model

1. Introduction

Irrigation modernisation in Indonesia is guided by a five-pillar approach covering water availability, irrigation infrastructure, irrigation management, irrigation institutions, and the people responsible for managing irrigation [1]. Sediment management is part of the infrastructure pillar because sediment entering irrigation networks can reduce canal discharge capacity [2], increase canal roughness through vegetation growth [3], and increase operation and maintenance (O&M) requirements, including dredging and cleaning [2,3]. Approximately 46% of Indonesia's irrigation infrastructure was reported to be moderately to heavily damaged based on 2018 data, highlighting the continuing challenges in maintaining irrigation systems [4]. These challenges are particularly relevant in tropical volcanic watersheds, where high sediment yields can make sediment control facilities vulnerable to siltation and increase the need for effective flushing strategies [5,6].

Indonesia's Irrigation Design Criteria (KP-02 and KP-04) provide design guidance for sediment control facilities in irrigation systems [7]. However, the applicability of this

Check for updates

Academic Editor: Bommanna Krishnappan

Received: 27 September 2026
Revised: 28 October 2026
Accepted: 30 October 2026
Published: 4 November 2026

Copyright: © 2026 by the authors. Licensee MDPI, Basel, Switzerland. This article is an open access article distributed under the terms and conditions of the Creative Commons Attribution (CC BY) license.

guidance to cohesive sediment at irrigation intakes requires further assessment. Previous research has investigated the trapping performance of vortex-tube sediment extractors and the design of tunnel-type sediment excluders for non-cohesive riverbed material [8,9]. More recent studies have evaluated sediment-ejector performance using laboratory data and predictive models based on factors such as grain size, settling velocity, sediment concentration, and extraction ratio [10]. Other work has examined desilting channels equipped with swirling flow generators, reporting trapping performance for sand-sized particles [11]. These studies provide useful design and operational references, but their findings do not by themselves establish the effectiveness of existing structures for cohesive sediment. The sediment excluder at Warujayeng Irrigation Area (IA), Nganjuk Regency, provides a relevant example of a KP-04 facility for investigating this issue.

Previous investigations of sediment in irrigation canals have examined sediment deposition thickness under different discharges and sediment concentrations [12], the role of sediment in irrigation canal design and management [2,13], mathematical modelling of sediment transport in Indonesian [14], non-uniform sediment transport [15], and the relationship between sediment transport and irrigation channel O&M [16]. Cohesive sediment introduces additional challenges because its transport and deposition depend on material properties and operating conditions. Osman reported that improved continuous operation could reduce cohesive-sediment deposition by up to 55% compared with a storage system [17]. Research on gate operation in irrigation canals has also demonstrated the potential for intermittent gate opening and closing to reduce sediment-related problems under certain operating conditions [18]. However, cohesive-sediment transport remains difficult to predict because erosion and deposition thresholds and flocculation parameters are often determined empirically and require consideration of local sediment characteristics [19].

The distinction between cohesive and non-cohesive sediment is also important when interpreting settling behaviour. For non-cohesive sediment, bed load is transported close to the bed, whereas suspended sediment remains in the water column through the balance between particle settling and turbulent mixing. The Rouse number provides a framework for describing the vertical concentration profile of suspended sediment and is expressed as:

$$P = \frac{w_s}{k u_*} \tag{1}$$

where P is the dimensionless Rouse number, w_s is the particle settling velocity, k is the von Kármán constant (approximately 0.41), and u_* is the shear velocity. A higher Rouse number indicates a greater tendency for particles to settle relative to turbulent mixing, whereas a lower value indicates a greater tendency to remain suspended. This framework must be applied cautiously to fine cohesive sediment because flocculation can alter effective particle size and settling velocity [19–21], while consolidation can increase the erosion resistance of deposited sediment [22]. Consequently, grain size and hydraulic conditions alone are insufficient to characterise cohesive-sediment deposition. In the present study, Rouse number similarity informs the planned sediment scaling approach for the physical model; it does not establish a validated field-scale cohesive-sediment concentration profile or trapping efficiency.

Numerical modelling can help investigate the complex flow and sediment patterns associated with cohesive material. Theol used Delft3D to examine cohesive and non-cohesive sediment deposition in irrigation systems and reported sensitivity to discharge and velocity, including asymmetric deposition around structures [23]. Three-dimensional numerical modelling has also been applied to hydrodynamics and cohesive-sediment transport in natural water bodies [24]. In freshwater rivers, fine silt and clay can form flocs whose settling behaviour differs from that of individual primary particles [20]. These

processes complicate direct prediction of cohesive-sediment settling and reinforce the need to distinguish hydraulic model validation from validation of sediment transport.

Research on sediment control structures provides additional design concepts but also identifies limitations in transferring results between sediment types and operating conditions. McLeod et al. investigated a distributed sediment excluder sand trap using numerical and field-based approaches and examined flow and sediment concentration distribution in a split-and-settle sand trap using physical and numerical modelling [25,26]. In the latter configuration, the splitter plate produced an approximately 60/40 discharge division, with sediment concentration beneath the plate reported to be 80% higher [26]. The distributed sediment excluder study reported trapping and flushing efficiencies of 27% and 36% under the evaluated low-discharge conditions, with higher values projected for modified configurations [25]. Separately, three-dimensional modelling has been used to investigate sediment deposition and erosion in reservoirs [27]. Studies of sand traps have further examined the influence of design, hydraulic conditions, sediment characteristics, and operational practices on performance [6,28,29]. Nevertheless, these findings cannot be directly interpreted as evidence of equivalent performance for cohesive sediment. Fine cohesive particles can flocculate, changing their effective settling behaviour [20,21], while consolidation can increase the critical shear stress required to erode deposited material [22].

Taken together, the design criteria and previous studies indicate a need to investigate sediment control configurations specifically in the context of cohesive sediment at irrigation intakes. This study therefore investigates a modified four-channel silt settler as a candidate configuration for managing cohesive sediment, using field observations from the Warujayeng sediment excluder and the existing sand trap at Tami Weir in Koya Tami IA, Jayapura, to establish the practical problem context. This study has three objectives: (1) to examine sediment conditions at the existing Warujayeng and Tami facilities; (2) to investigate flow, sediment load distribution, and potential settling and flushing behaviour through numerical simulations and hydraulic physical model testing; and (3) to assess the modified silt settler configuration as a reference for further prototype development. This study combines field observations and sediment analyses, HEC-RAS 2D modelling of existing conditions, FLOW-3D Hydro simulations of two four-channel alternatives (2A and 2B), a threshold-based assessment of settling opportunity, and hydraulic validation using a 1:5 physical model. Because the numerical sediment formulation does not fully represent cohesive-sediment behaviour, the results are interpreted as comparative model indicators rather than validated predictions of field-scale cohesive-sediment trapping efficiency. The contribution is therefore the evaluation of a modified configuration and its hydraulic and settling-related indicators as a basis for further investigation, rather than the demonstration of a fully validated cohesive-sediment excluder.

2. Materials and Methods

2.1. Study Sites

This study was conducted at three sites. The first site was the Warujayeng Main Canal, supplied by the left intake of the Mrican Barrage (Brantas River), Nganjuk Regency, East Java, with a command area of 12,491 ha of paddy fields and a designed discharge of 15,996 L/s; the desilting basin and sediment excluder at this site were the reference examples in KP-04 and were flushed routinely once a month. The second site was Tami Weir in Muara Tami District, Jayapura City, Papua (Figure 1), built in the early 1990s to irrigate the 5000 ha Koya IA. This fixed weir has a seven-tooth labyrinth (saw-tooth) spillway, one scouring sluice, one intake with a capacity of 7.5 m^3/s (used as the flushing discharge; design settling discharge 5.0 m^3/s), two sand traps, and 74 tertiary blocks. Because sand trap flushing was ineffective, the Papua River Basin Organization (BWS Papua) added a second flushing gate

downstream of the sand trap. The third site was the Hydraulic Structures and Irrigation Laboratory, Institut Teknologi Bandung (ITB), Jatinangor Campus, where the physical model tests were conducted.

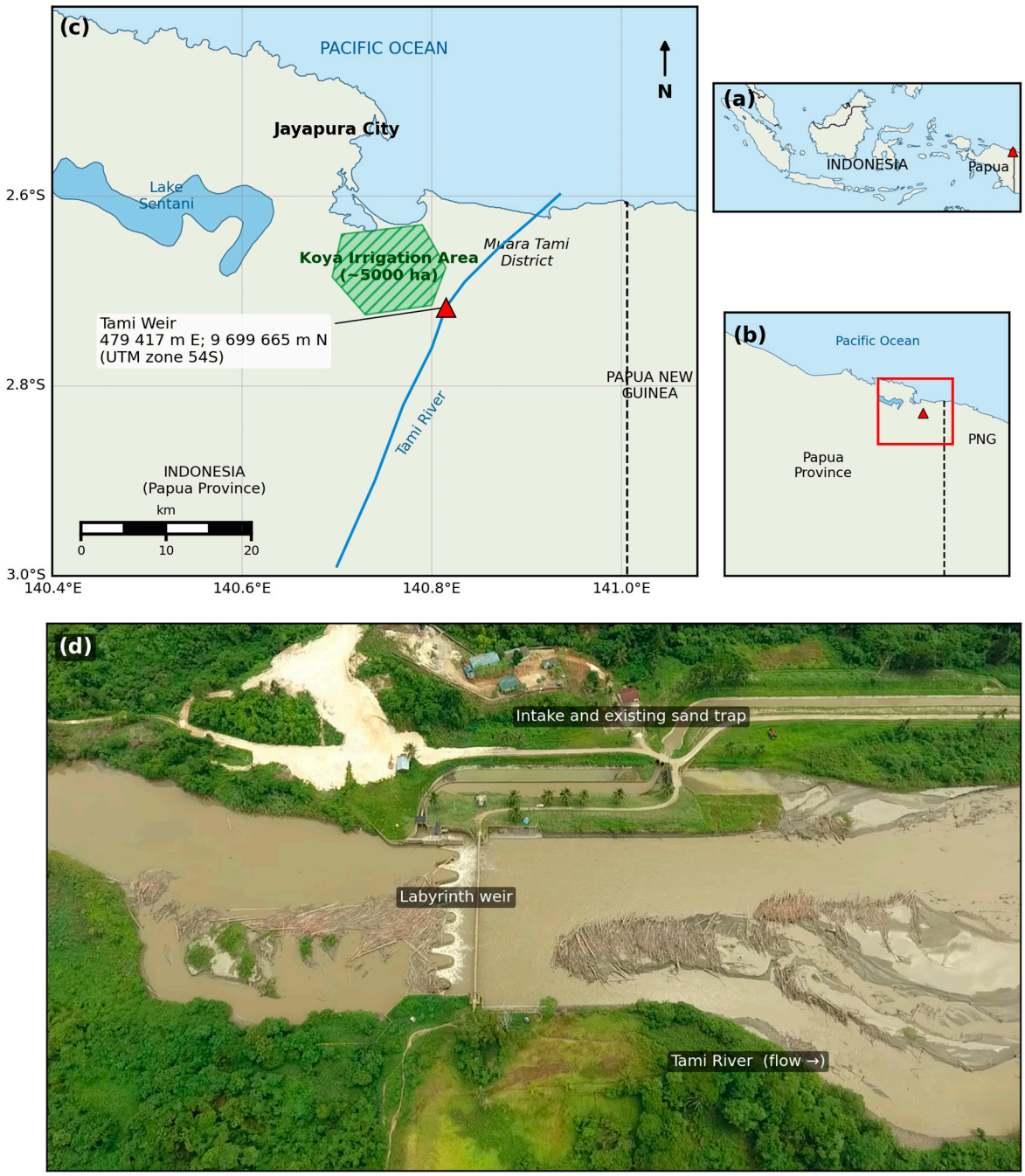


Figure 1. Location of Tami Weir and the Koya Irrigation Area, Muara Tami District, Jayapura City, Papua Province: (**a**) Indonesia; (**b**) northern Papua; (**c**) study area (irrigation-area outline approximate); (**d**) aerial view of Tami Weir, the intake, and the existing sand trap.

A field inspection in April 2026 showed sediment deposits filling the sand trap up to the flushing gate 2 structure and the main canal (Figure 2). Land cover change upstream also caused both the upstream and downstream sides of the weir to fill with sediment, making both flushing gates difficult to operate, and the deposits were removed manually with a backhoe.



Figure 2. Accumulation of cohesive sediment in main canal and sand trap of Tami Weir (documentation, April 2026).

2.2. Sediment Sampling and Analysis

At Warujayeng IA, two sediment samples were taken in the main canal downstream of the sediment excluder (June 2025) to identify the type of sediment passing the structure. At Koya Tami IA, bedload and suspended load samples were taken at three locations, namely, the Tami River channel near the intake (Location 1), the sand trap (Location 2), and the irrigation canal downstream of the sand trap (Location 3), with two samples each. Sampling involved grab sampling and core sampling, and the suspended load was sampled by depth-integrated sampling. Laboratory analyses comprised specific gravity, sieve and hydrometer analyses for material passing 0.075 mm according to ASTM, and total suspended solids (TSSs). Gradation was classified according to the Wentworth scale, namely, clay < 0.002 mm and silt 0.002–0.0625 mm.

2.3. HEC-RAS 2D Modelling of Existing Sand Trap

The performance of the existing sand trap was evaluated with the two-dimensional sediment transport module of HEC-RAS version 6.6 [30], which has been applied to model long-term sediment accumulation in a reservoir in Indonesia [31]. The computational domain was an unstructured mesh with a cell size of 0.4 m in the main channel and 0.2 m along the side walls and canal edges. Manning coefficients of 0.025–0.030 were calibrated against velocity and water-level measurements [29]. Cohesive sediment transport was modelled with the Partheniades erosion function [32] and the Krone deposition method [33], with a median grain size of about 12 μm as the dominant suspended load fraction and an initial bed material thickness of 1.5 m. The upstream sediment boundary condition was a concentration of 220 mg/L at 5.0 m3/s and 250 mg/L at 7.5 m3/s, within the measured TSS range of 130–270 mg/L, with an inflow gradation of 28% clay, 31% medium silt, and 41% coarse silt. This Krone–Partheniades approach has proven decisive in simulating fine sediment retention with HEC-RAS [34], and its parameters need to be adjusted to local sediment properties [19]. The erosion rate was calculated as:

$$E = M\,(\tau_b/\tau_c - 1) \tag{2}$$

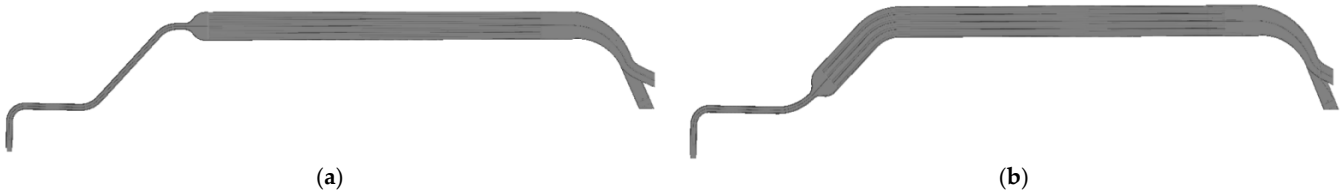
where E is the erosion rate, M the erodibility coefficient, τ_b the bed shear stress, and τ_c the critical shear stress for erosion. Partheniades [32] gives τ_c values of 0.10–0.15 N/m^2 for soft unconsolidated silt (D_{50} 0.010–0.020 mm), 0.15–0.30 N/m^2 for moderately consolidated silt (D_{50} 0.020–0.050 mm), and 0.30–0.50 N/m^2 for well-consolidated cohesive beds (D_{50} 0.030–0.060 mm). Based on field observations showing a predominance of moderately consolidated fine silt, $\tau_c = 0.20$ N/m^2 was used. This choice considers that the erosion threshold of mud deposits is mainly controlled by their dry bulk density, which increases with consolidation [22]. The hydraulic and sediment time steps were set to 10 s with a

continuous simulation duration of 30 days, at discharges of 7.5 m^3/s (maximum intake capacity) and 9 m^3/s (120% of capacity, as a capacity test). Trapping efficiency was calculated from the incoming (M_{in}) and outgoing (M_{out}) sediment mass:

$$TE\ (\%) = (M_{in} - M_{out})/M_{in} \times 100 \quad (3)$$

2.4. Silt Settler Design Concept and FLOW-3D Hydro Simulation

Two silt settler alternatives were designed for Koya Tami IA (Figure 3). Alternative 2A converts the existing sand trap into a feeder canal from the intake gate and then provides a straight silt settler up to a new flushing structure upstream of flushing gate 2. Alternative 2B modifies the existing sand trap and part of the main canal following the site contours (curved at the start and then straight) without changing the intake gate and approach channel, with a new flushing structure at the same location. Both alternatives consist of four compartments (channels), with the central part, one-third of the structure width, made deeper so that cohesive sediment accumulates there.



(**a**) (**b**)

Figure 3. Three-dimensional geometry of FLOW-3D Hydro model: (**a**) Alternative 2A; (**b**) Alternative 2B.

The simulations were performed with FLOW-3D Hydro 2025R1 (Flow Science, Inc., Santa Fe, NM, USA), which solves the continuity and non-hydrostatic three-dimensional Reynolds-averaged Navier–Stokes (RANS) equations on a structured rectangular grid with the FAVOR™ method, tracks the free surface with TruVOF, and uses the RNG k–ε turbulence model. The combination of FLOW-3D, the RNG k–ε model, and its sediment scour module has been validated against field data downstream of a barrage with $R^2 = 0.91$ and NSE = 0.90 [35]. The upstream boundary condition is a discharge (fluid rate) and the downstream boundary condition is outflow/pressure. Identical inflow, outflow, and sediment load conditions were applied to both alternatives. The sediment model parameters are presented in Table 1; the bedload transport rate was calculated with the Nielsen equation, and the bedload layer thickness follows the van Rijn formulation available in the FLOW-3D sediment module, which also provides the Soulsby–Whitehouse equation for the critical Shields parameter; the same entrainment coefficient of 0.018 was used in the FLOW-3D study by Zaffar et al. [35]. The simulation output grouped the ten size classes into four sediment species (Packed Sediment 1–4).

The FLOW-3D sediment model is non-cohesive and controls transport and deposition with a single Shields threshold, whereas the deposition of clay and silt only proceeds fully when the bed shear stress falls below the deposition threshold $\tau_d = 0.03$–$0.10\ N/m^2$ [33], and erosion of cohesive deposits only starts above the erosion threshold $\tau_e \approx 0.20\ N/m^2$ [32]. Cohesive behaviour was therefore assessed in post-processing with $\tau_d = 0.06\ N/m^2$ and $\tau_e = 0.20\ N/m^2$. Performance is not expressed as a single trapping efficiency but as a settling opportunity index, i.e., the fraction of sediment transport exposure occurring over a bed with a shear stress lower than τ_d:

$$I_s = \int q_s(x) \cdot 1[\tau_b(x) < \tau_d]\, dx / \int q_s(x)\, dx \quad (4)$$

where q_s is the sediment flux per unit width, and the integral is taken along the channel, so the index does not depend on the choice of measurement points. The distinction between

the simulated sediment transport and the interpretation of cohesive-sediment behaviour is important. FLOW-3D Hydro was used to calculate the flow field and sediment transport for its specified non-cohesive sediment classes. Cohesive behaviour was not explicitly represented by the sediment transport formulation; instead, the simulated bed-shear-stress field was assessed in post-processing against deposition and erosion thresholds adopted from the literature. These thresholds were not calibrated using site-specific cohesive-sediment erosion or deposition tests. Accordingly, the settling opportunity index indicates the proportion of the simulated transport exposure occurring under bed-shear-stress conditions below the selected deposition threshold. It is a conditional indicator of potential settling opportunity, not a direct prediction or measurement of cohesive-sediment trapping efficiency.

Table 1. Sediment transport model parameters in FLOW-3D Hydro.

Parameter	Value
Number of sediment size classes	10 equally spaced classes, 0.0300–0.0625 mm
Grain density	2.650 kg/m^3
Critical Shields parameter	Soulsby–Whitehouse equation, with slope correction
Bedload transport equation (coefficient)	Nielsen (12)
Entrainment coefficient	0.018
Angle of repose	32°
Maximum packing fraction	0.64
Richardson–Zaki coefficient multiplier	1
Turbulent diffusion multiplier	1.43
Bed roughness/d_{50} ratio	2.5
Settling discharge/flushing discharge	5.0 m^3/s/7.5 m^3/s

Data were taken from sampling points along the centreline of the four channels (depth, depth-averaged velocity, bed shear stress, and sediment concentration). Because the wall shear stress column was resolved at only 150 of 403 points (8 of 204 points in Alternative 2A and 142 of 199 points in Alternative 2B), the bed shear stress of both alternatives was estimated with a single relationship calibrated on those 150 points ($R^2 = 0.768$; $C_f = 7.2 \times 10^{-4}$; equivalent to Manning ≈ 0.009):

$$\tau_b = 0.7198\, U^2 \quad (5)$$

where U is the depth-averaged velocity (m/s). The bed-shear-stress relationship should be interpreted as an approximate estimator rather than an independently validated representation of bed resistance across both alternatives. The available wall shear-stress data were unevenly distributed between Alternative 2A and Alternative 2B, with only 8 of 204 points available for Alternative 2A and 142 of 199 points for Alternative 2B. Consequently, the pooled regression may be more representative of the sampled conditions in Alternative 2B than those in Alternative 2A. The equivalent Manning coefficient inferred from this relationship is not treated as a calibrated channel-roughness coefficient; it is reported only as an equivalent value associated with the fitted relationship. Because the settling opportunity index depends directly on the estimated bed shear stress and the selected deposition threshold, comparisons between alternatives are conditional on this approximation and require further verification using more balanced spatial sampling or directly resolved bed shear-stress data. The surface loading rate was calculated as $q = U{\cdot}h/L$ (h flow depth, L channel length) and compared with the designed rule for fine-sediment sand traps of 0.5–1.5 m/h. The sensitivity of the results was tested at $\tau_d = 0.03$, 0.06, 0.10, and 0.15 N/m^2. This sensitivity assessment is important because changing the deposition threshold changes the proportion of the simulated transport exposure classified as a settling opportunity. Accordingly, the resulting index and the relative ranking of the alternatives should

be interpreted in relation to the selected threshold rather than as threshold-independent performance measures. The effect of flocculation was examined with the Krone rule [33] and the van Leussen turbulence correction [36]:

$$w_s = k \cdot C^m \quad (6)$$

where w_s is the floc settling velocity, C the sediment concentration, and k and m empirical coefficients. Alternative 2A was then optimised with flow-conditioning baffles at the channel inlet (volume 32.46 m^3, open surface area 59.08 m^2); the baffled model under normal operation was run up to 2.500 s. Flushing with the baffled model was simulated at a discharge of 7.5 m^3/s (150% of the settling discharge) for two scenarios, namely, one-gate (side) opening and full (two-gate) opening, with durations of 683.0 and 679.0 s. The flushing mass balance was closed by integrating the sediment mass flow rate at the outlet flux plane over the real simulation time (output interval 1.000 s).

2.5. Physical Model Tests at 1:5 Scale

An undistorted 1:5 scale physical model was built at the Hydraulic Structures and Irrigation Laboratory, ITB Jatinangor (Figure 4), with Froude similarity, because open-channel flow is dominated by gravity. The parameter scales and model discharges are presented in Table 2. Velocity was measured with a 16 MHz down-looking micro acoustic Doppler velocimeter (MicroADV) and a 10 MHz side-looking ADV (SonTek, a Xylem brand, San Diego, CA, USA), with data recorded using HorizonADV software (v1.20; SonTek/YSI, San Diego, CA, USA) at 50 Hz for 30–60 s per point; water levels were measured with point gauges; inflow was measured with a laboratory flow meter and outflow with a Thomson V-notch weir fabricated in the laboratory.



Figure 4. The 1:5 scale physical silt settler model at the Hydraulic Structures and Irrigation Laboratory, ITB Jatinangor Campus, during hydraulic flow testing.

Sediment scaling was based on Rouse number similarity, $P = w_s/(ku_*)$, because the focus of this study was the settling of suspended sediment. Shear velocity follows Froude scaling, so the model settling velocity had to be reduced by a factor of 2.236. Table 3 compares the scaling options; Option A was selected (same material, model diameter 0.050 mm, achievable with fine silica flour). Rouse number similarity cannot be satisfied simultaneously with Shields parameter similarity, and this is a stated limitation of the tests.

Because the available flume was 60 m long, the model represented the upstream 300 m of the structure while retaining the 1:5 scale.

Table 2. Hydraulic parameter scales and discharges of 1:5 physical model (Froude similarity, $n_L = 5$).

Parameter	Scale Formula	Scale Value	Prototype	Model
Length, height	$n_L = n_h$	5	—	—
Time, velocity	$n_L^{1/2}$	2.236	—	—
Discharge	$n_L^{5/2}$	55.902	—	—
Manning coefficient	$n_L^{1/6}$	1.308	—	—
Settling velocity	$n_L^{1/2}$	2.236	—	—
Discharge Q50%	—	—	2.5 m^3/s	44.72 L/s
Discharge Q100% (settling)	—	—	5.0 m^3/s	89.44 L/s
Discharge Q120%	—	—	6.0 m^3/s	107.33 L/s
Flushing discharge	—	—	7.5 m^3/s	134.16 L/s
Length × width, Alternative 2A	—	—	331.96 × 27.5 m	66.4 × 5.5 m
Length × width, Alternative 2B	—	—	408–423 × 27.5 m	81.6–84.6 × 5.5 m

Table 3. Basic check of sediment scaling for 1:5 physical model (prototype diameter 0.075 mm; prototype w_s 5.04 mm/s).

Scaling Basis	d Model (mm)	Relative Density	w_s Model (mm/s)	Rouse Model/Prototype	Assessment
$n_d = n_L^{3/2}$ (original)	0.0067	2.65	0.040	0.018	Unsuitable; model practically does not settle
Same material without scaling	0.075	2.65	5.038	2.236	Unsuitable; excessive settling by a factor of ±2
Option A: same material, reduced grain size	0.050	2.65	2.253	1.000	Recommended (fine silica flour)
Option B: same grain size, lighter material	0.075	1.74	2.253	1.000	Recommended if available (e.g., fine anthracite)

Hydraulic validation (series 0, without sediment) compared the FLOW-3D results with the physical model at 69 water-level points and 23 velocity points (inlet, four lanes A–D, and outlet) at Q50%, Q100%, and Q120% discharges (2.5, 5.0, and 6.0 m^3/s prototype). Agreement was assessed with the mean absolute error (MAE, in percent of the measured value), the root mean square error (RMSE), and the percent bias (PBIAS). Sediment transport tests in the physical model are still in progress and are not included in this article. The assumptions underlying the physical model tests defined the scope of their applicability. Froude similarity was adopted to reproduce the gravity-dominated free-surface hydraulic behaviour at a geometric scale of 1:5. For sediment scaling, Rouse number similarity was selected to approximate the balance between particle settling and turbulent mixing. However, Rouse number similarity cannot be satisfied simultaneously with Shields parameter similarity under the selected scaling conditions. Therefore, the physical model does not achieve complete dynamic similarity for sediment transport, erosion, and deposition. In particular, the hydraulic validation reported in this study does not validate cohesive-sediment transport or trapping efficiency. The physical model results

were consequently used to assess hydraulic behaviour under the tested conditions, while sediment transport performance requires separate physical testing and further verification.

3. Results

3.1. Sediment Characteristics and Performance of Warujayeng IA Sediment Excluder

The sediment excluder structure at Warujayeng IA is not visible in the field because it lies at the canal bed. Both samples downstream of the structure were classified as clayey silt with a silt and clay fraction of more than 95% (Table 4). These findings show that fine-grained sediment was present downstream of the structure; however, without upstream samples, the sediment excluder's retention efficiency could not be determined. Because upstream samples were not yet available, the efficiency of the structure could not be quantified.

Table 4. Composition of main canal sediment downstream of Warujayeng IA sediment excluder (June 2025).

Fraction	Sample 1 (%)	Sample 2 (%)
Gravel	0.00	0.00
Sand	4.02	3.62
Silt	75.01	74.59
Clay	20.97	21.79
Soil type	Clayey silt	Clayey silt

Sediment at Koya Tami IA was even finer (Table 5). The bedload in the Tami River channel (Location 1) contained on average 60% silt and 17% clay (cohesive fraction 77%), with a mean specific gravity of 2.462 and a TSS of 269.5 mg/L. In the sand trap (Location 2), the cohesive fraction reached 97% (silt 46.47%, clay 51.5%), with a specific gravity of 2.346 and TSSs of 130 mg/L, whereas in the canal downstream of the sand trap (Location 3), the entire bedload was cohesive (silt 58%, clay 42%), with a specific gravity of 2.430 and a mean TSS of 133 mg/L.

Table 5. Laboratory results for Koya Tami IA sediment (June 2025).

Parameter	Location 1: Tami River Channel Near the Intake		Location 2: Sand Trap		Location 3: Canal Downstream of the Sand Trap	
Sample depth (m)	4.00	3.50	1.10	1.10	0.44	0.44
Specific gravity (–)	2.433	2.491	2.285	2.407	2.423	2.437
Passing sieve #200 (%)	64.76	69.29	95.23	99.25	99.58	99.42
Gravel (%)	0.00	0.02	0.03	0.01	0.00	0.00
Sand (%)	26.00	19.98	3.97	0.06	0.02	0.00
Silt (%)	55.00	65.00	35.00	57.93	57.98	58.00
Clay (%)	19.00	15.00	61.00	42.00	42.00	42.00
Suspended load TSS (mg/L)	239	300	76	184	114	152

Notes: Parameters from depth to clay were from bedload samples; TSSs were from suspended load samples at the same depth.

3.2. Performance of the Existing Tami Weir Sand Trap

The HEC-RAS longitudinal profile shows that the water levels at discharges of 7.5 and 9 m^3/s remained well below the bank elevation of 44 m, so the sand trap was not at risk of overtopping. Velocities at the inlet ranged from 0.8 to 1.0 m/s and decreased to

below 0.2 m/s in the middle of the basin; high velocities occurred at the left-side bend, with potential for local scour. Along the sand trap axis, the velocity decreased from about 0.8 m/s upstream to below 0.1 m/s in the 40–100 m segment, which formed the main deposition zone (Figure 5a). However, the flow never fully stopped, so cohesive particles requiring long settling times remained partly in suspension.

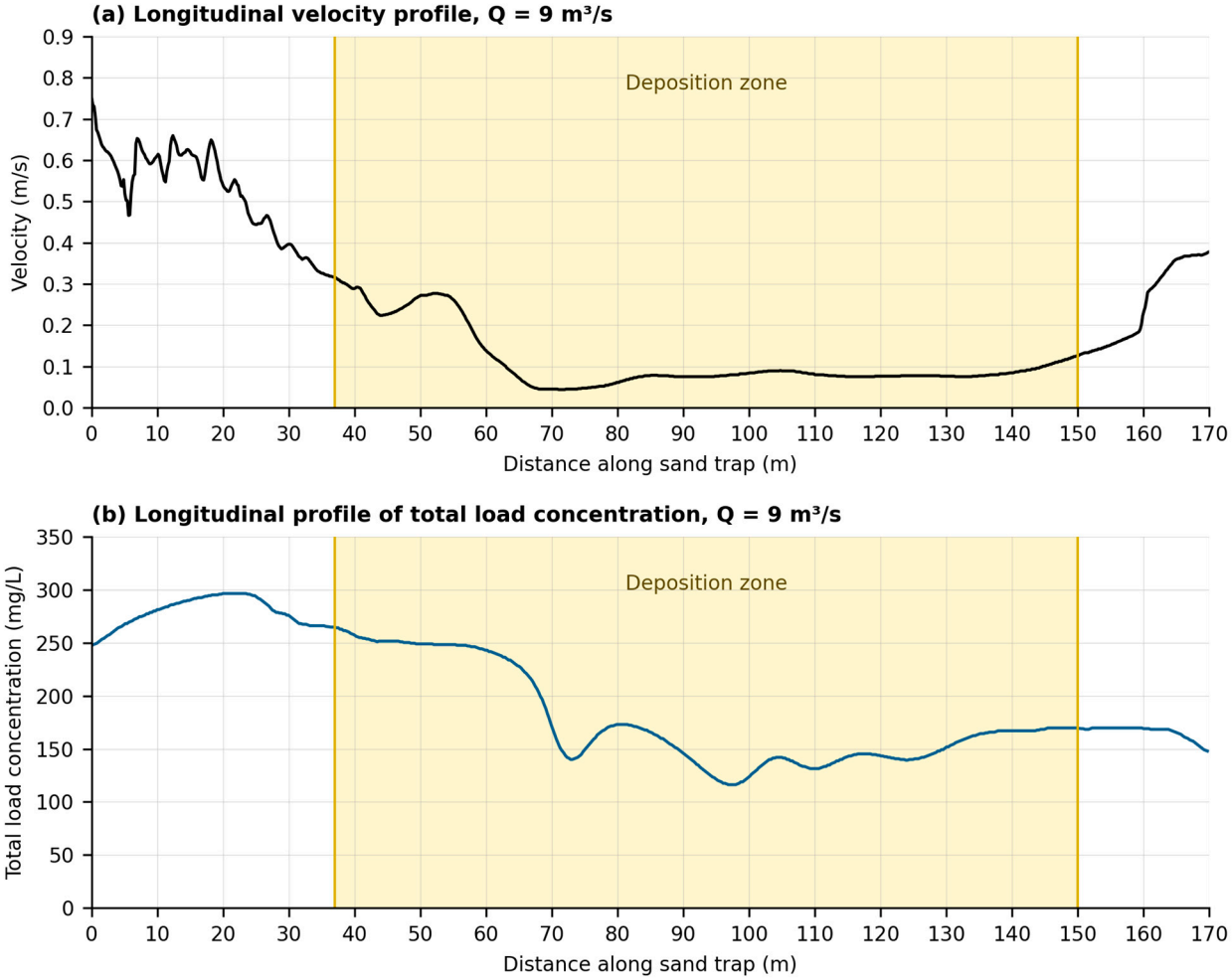


Figure 5. HEC-RAS 2D results for existing Tami Weir sand trap at discharge of 9 m^3/s: (**a**) longitudinal velocity profile; (**b**) longitudinal profile of total load concentration. The yellow lines delimit the deposition zone.

The sediment concentration in the two-dimensional map decreased from 380–427 mg/L upstream to 200–250 mg/L in the middle of the sand trap, where $\tau_b < \tau_c$ promotes flocculation and deposition. At the test discharge of 9 m^3/s (Figure 5b), the concentration reached about 300 mg/L near the inlet due to turbulence and local resuspension, decreased markedly at 40–100 m, and stabilised at about 150 mg/L downstream. For the 5.0 m^3/s simulation, the mass-based trapping efficiency of the existing sand trap was only about 27% (the total concentration decreased from 220 mg/L at the in-flow boundary to 161 mg/L at the downstream boundary), almost entirely from coarse silt (47%), compared with 20% for medium silt and 5% for clay, and the remainder passed into the irrigation canal.

3.3. Flow Field and Settling Opportunity of Alternatives 2A and 2B

In Alternative 2A, the flow is concentrated as a velocity core in the central channels from the inlet to the outlet, whereas the side channels have much lower velocities; suspended sediment and deposits are concentrated mainly in channels 2 and 3 (Figure 6a). Alternative

2B produces a wider flow spread with a smaller peak-velocity region, although the central channels still carry a higher proportion of sediment than channels 1 and 4 (Figure 6b).

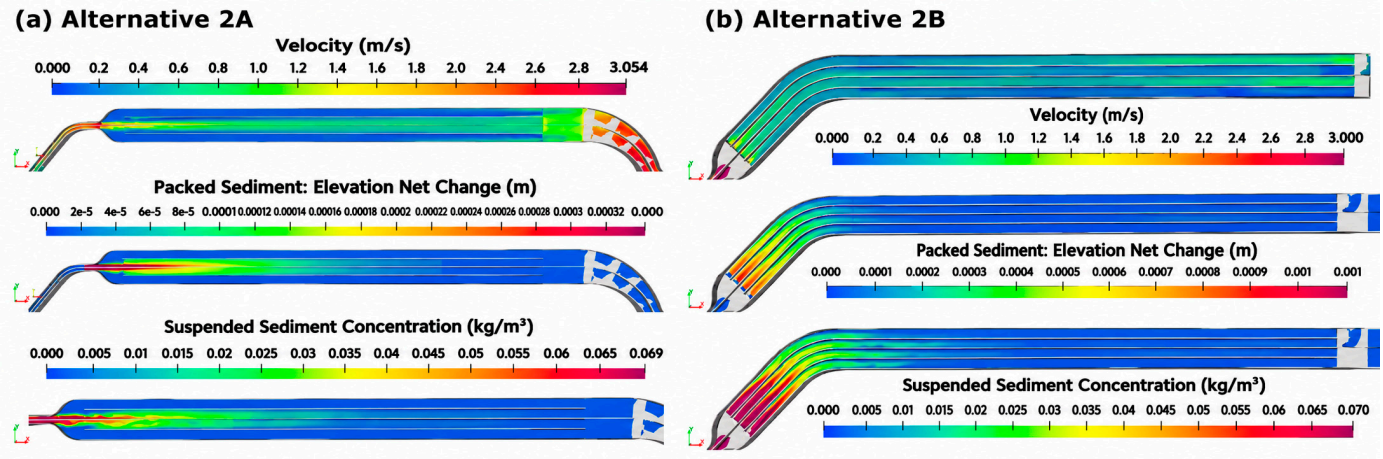


Figure 6. FLOW-3D Hydro results at settling discharge (t = 2250 s); from top to bottom: flow velocity, change in deposited sediment elevation, and suspended sediment concentration. (**a**) Alternative 2A; (**b**) Alternative 2B.

The measured hydraulic quantities of both alternatives are presented in Table 6. The most important item is the surface loading rate: 2.38–8.14 m/h for Alternative 2A and 2.19–3.59 m/h for Alternative 2B, both far above the 0.5–1.5 m/h rule for fine sediment. The minimum settling velocity required for particles to reach the bed before leaving is 0.61–2.26 mm/s, whereas, according to Stokes' law, the 12 µm field grains settle at only about 0.13 mm/s; the 0.03 and 0.0625 mm model grains settle at about 0.81 and 3.50 mm/s. The simulation results therefore represent the coarse silt fraction and constitute an upper bound for sediment of field D_{50} size.

Table 6. Measured hydraulic quantities of two designed alternatives at settling discharge of 5.0 m^3/s.

Quantity	Alternative 2A	Alternative 2B	Remarks
Channel length	331.96 m	408–423 m	2B path 23–27% longer
Mean flow depth	1.26–1.28 m	0.76–0.90 m	2B shallower
Mean velocity	0.17–0.59 m/s	0.32–0.51 m/s	2A split into two groups; 2B more uniform
Hydraulic residence time	9.4–31.8 min	13.5–21.6 min	2A range very wide
Median bed shear stress	0.019–0.267 N/m^2	0.056–0.180 N/m^2	Estimated with Equation (5)
Channel length below $\tau_d = 0.06$ N/m^2 (ch. 1/2/3/4)	99.6/0/0/99.2%	0/31.0/0/50.7%	2A sharply split; 2B around the threshold
Surface loading rate $q = U{\cdot}h/L$	2.38–8.14 m/h	2.19–3.59 m/h	Fine-sediment rule 0.5–1.5 m/h
Minimum settling velocity	0.66–2.26 mm/s	0.61–1.00 mm/s	For particles to reach the bed before leaving

This difference in particle size and settling velocity limits the representativeness of the sediment transport results for the field conditions. The simulated classes settle substantially faster than the reported 12 µm field fraction and therefore cannot reproduce its settling behaviour directly. In addition, the simulations did not explicitly resolve cohesive floc formation, changes in floc settling velocity, or the consolidation-dependent increase in erosion resistance. The results should therefore be interpreted as a comparative assessment

of flow and potential settling conditions under the specified modelling assumptions, rather than as quantitative predictions of field-scale cohesive-sediment deposition.

The settling opportunity index (Table 7) reveals the different natures of the two alternatives. Alternative 2A is sharply split: channels 1 and 4 flow at 0.17 and 0.19 m/s with shear stresses of 0.019 and 0.021 N/m^2, giving indices of 90.27% and 84.24%, whereas channels 2 and 3 flow at 0.56 and 0.59 m/s with shear stresses of 0.25 and 0.27 N/m^2 (above the erosion threshold), giving indices of zero. Yet these two zero-index channels receive 99.5% of the sediment transport exposure, so the system index is only 0.48%. Alternative 2B distributes the load more evenly (30.7:38.5:19.1:11.7%), but all its channels have shear stresses of 0.056–0.180 N/m^2, above the deposition threshold, so its system index is only 0.02% with a ceiling of 0.08%, whereas the ceiling of Alternative 2A reaches 87.26%.

Table 7. Settling opportunity index and share of sediment transport exposure per channel ($\tau_d = 0.06$ N/m^2).

Position	Index 2A (%)	Exposure Share 2A (%)	Index 2B (%)	Exposure Share 2B (%)
Channel 1	90.27	0.3	0.00	30.7
Channel 2	0.00	45.8	0.00	38.5
Channel 3	0.00	53.7	0.00	19.1
Channel 4	84.24	0.3	0.16	11.7
System index	0.48	—	0.02	—
If exposure is uniform (25%)	43.63	—	0.04	—
Ceiling (two quietest channels)	87.26	—	0.08	—

The ranking of the two alternatives is sensitive to the selected deposition threshold. At τd = 0.03 and 0.06 N/m^2, Alternative 2A yields higher settling opportunity indices than Alternative 2B (0.43% and 0.48% versus 0.001% and 0.02%, respectively). However, at τd = 0.10 and 0.15 N/m^2, the ranking reverses, with Alternative 2B yielding indices of 2.16% and 18.32% compared with 1.56% and 1.80% for Alternative 2A. These changes indicate that the relative performance of the alternatives cannot be considered robust to the selected threshold. Moreover, the estimated bed shear-stress relationship was calibrated using an uneven distribution of available data points between the two alternatives, which introduced an additional source of uncertainty into the calculated indices and their comparison. The results should therefore be interpreted as conditional diagnostic estimates rather than definitive evidence that one alternative provides superior cohesive-sediment trapping. For Alternative 2B, the simulated deposition profile indicates that half of the deposited mass occurs within the first 27–34 m and nine-tenths within the first 82–109 m. This spatial pattern suggests that deposition is concentrated in part of the structure length under the modelled conditions (Figure 7); it does not independently establish field-scale cohesive-sediment performance.

Flocculation cannot be relied upon to increase deposition. Using Equation (6) and the van Leussen correction, the maximum enhancement in settling velocity is only 1.21 times at an optimum velocity gradient of $G = 1.38$ s^{-1} and returns to unity at $G = 3.33$ s^{-1}. Flocculation only becomes significant at concentrations of 599–1.530 mg/L, whereas the simulated concentrations are only 81–142 mg/L. With the applied flocculation correction, the model-based settling-efficiency estimates range from 1.7% to 9.6% for Alternative 2B, whereas the estimated value for Alternative 2A remains close to zero. These estimates depend on the assumed settling-velocity relationship and the simulated sediment concentrations and should not be interpreted as validated field-scale cohesive-sediment trapping efficiencies.

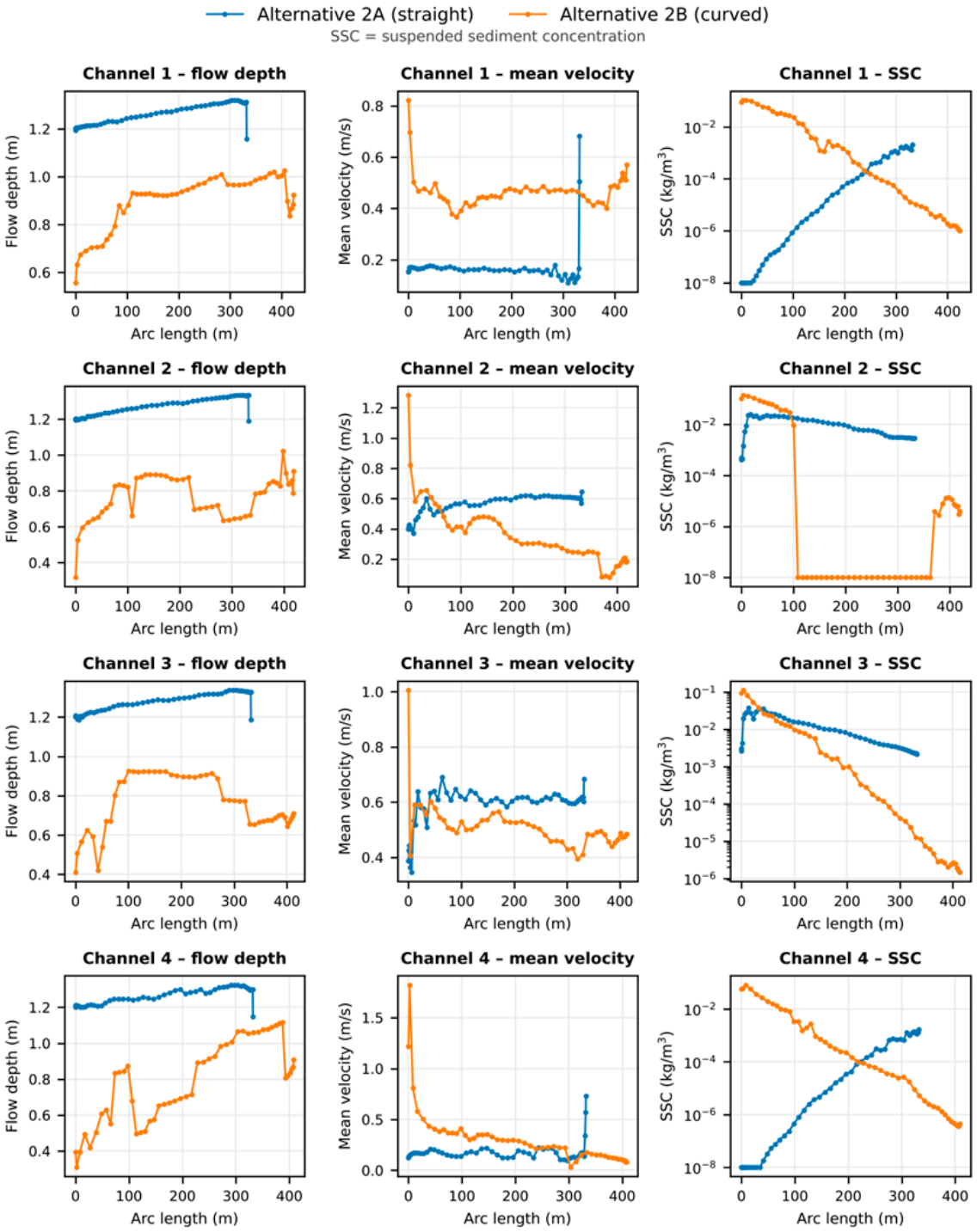


Figure 7. Comparison of longitudinal profiles of flow depth, mean velocity, and suspended sediment concentration in four channels of Alternatives 2A and 2B.

3.4. Effect of Baffles at Inlet of Alternative 2A

Baffles at the channel inlet break up the momentum of the central jet and even out the flow distribution among the four channels. Their effect was measured directly because both flushing simulations were run with the baffled model (Table 8). The coefficient of variation of load distribution decreased from 1.474 to 0.331 and 0.297, or about 4.5 times more uniform. Channels 1 and 4, which previously received no load, now receive about 34 and 31%, and these are precisely the channels with the highest settling opportunity index. These results indicate that the inlet baffles improved the distribution of simulated

sediment load among the four channels under the tested flushing conditions. However, the more uniform distribution does not by itself demonstrate improved cohesive-sediment trapping efficiency, because the channel load shares were obtained at a flushing discharge of 7.5 m^3/s, whereas the channel-specific settling opportunity indices were calculated at a settling discharge of 5.0 m^3/s.

Table 8. Distribution of sediment load among channels without and with baffles.

Condition	Ch. 1 (%)	Ch. 2 (%)	Ch. 3 (%)	Ch. 4 (%)	Coefficient of Variation
Alternative 2A without baffles	0.0	11.7	88.3	0.0	1.474
With baffles, 1-gate flushing	33.9	15.9	17.6	32.5	0.331
With baffles, 2-gate flushing	33.8	16.2	19.3	30.7	0.297
Alternative 2B without baffles (comparison)	27.6	32.4	20.1	19.9	0.211

When the channel load shares obtained from the baffled flushing simulations are applied to the per-channel settling opportunity indices of Alternative 2A, the projected system index increases from 0.48% to 56.37–58.04% (Table 9; Figure 8). This value is an exploratory upper-bound estimate rather than a validated performance measure because the load shares were obtained at a flushing discharge of 7.5 m^3/s, whereas the per-channel indices were calculated at a settling discharge of 5.0 m^3/s.

Table 9. Projected settling opportunity index of Alternative 2A under load distribution scenarios.

Load Distribution Scenario	Channel Share 1:2:3:4	Projected Index (%)
Alternative 2A without baffles	0.3:45.8:53.7:0.3	0.48
Assuming uniform exposure	25:25:25:25	43.63
With baffles (shares from 2-gate flushing)	33.8:16.2:19.3:30.7	56.37
With baffles (shares from 1-gate flushing)	33.9:15.9:17.6:32.5	58.04
Theoretical ceiling (entire load to channels 1 and 4)	50:0:0:50	87.26

3.5. Flushing Performance

At a flushing discharge of 7.5 m^3/s, the velocity along the main channels is relatively uniform at about 1.5 m/s. Full opening produces outlet velocities of 2–4 m/s, whereas one-gate opening produces only 0.5–2 m/s with a recirculation zone near the outlet channel. At the end of the simulation, the maximum bed lowering in all four channels is the same in both scenarios, namely, 0.117 m, with a remaining packed sediment volume fraction of about 0.007, so both scenarios reach a clean state.

The mass balance (Table 10; Figure 9) shows similar flushed sediment masses under the two scenarios: 246.2 t for one-gate opening and 248.4 t for full opening. The absolute difference is 2.2 t, equivalent to approximately 0.89% of the mass removed under one-gate opening. The total water volume used was 13,260 m^3 for one-gate opening and 12,538 m^3 for full opening, representing a reduction of 722 m^3, or approximately 5.44%, under full opening. The specific water use was 0.0539 m^3/kg (53.9 L/kg) and 0.0505 m^3/kg

(50.5 L/kg), respectively, a reduction of approximately 6.31%. These percentages were calculated from the reported values and were subject to rounding. Although the simulations indicate lower water use under full opening, the small difference in flushed sediment mass and the absence of an uncertainty analysis prevent a definitive conclusion that full opening provides a robust operational advantage. The results should therefore be interpreted as a comparison of the two simulated scenarios rather than as a validated operational recommendation. The four sediment species were transported in relatively similar proportions (22.6–27.2%), indicating limited grain-size sorting within the simulated range.

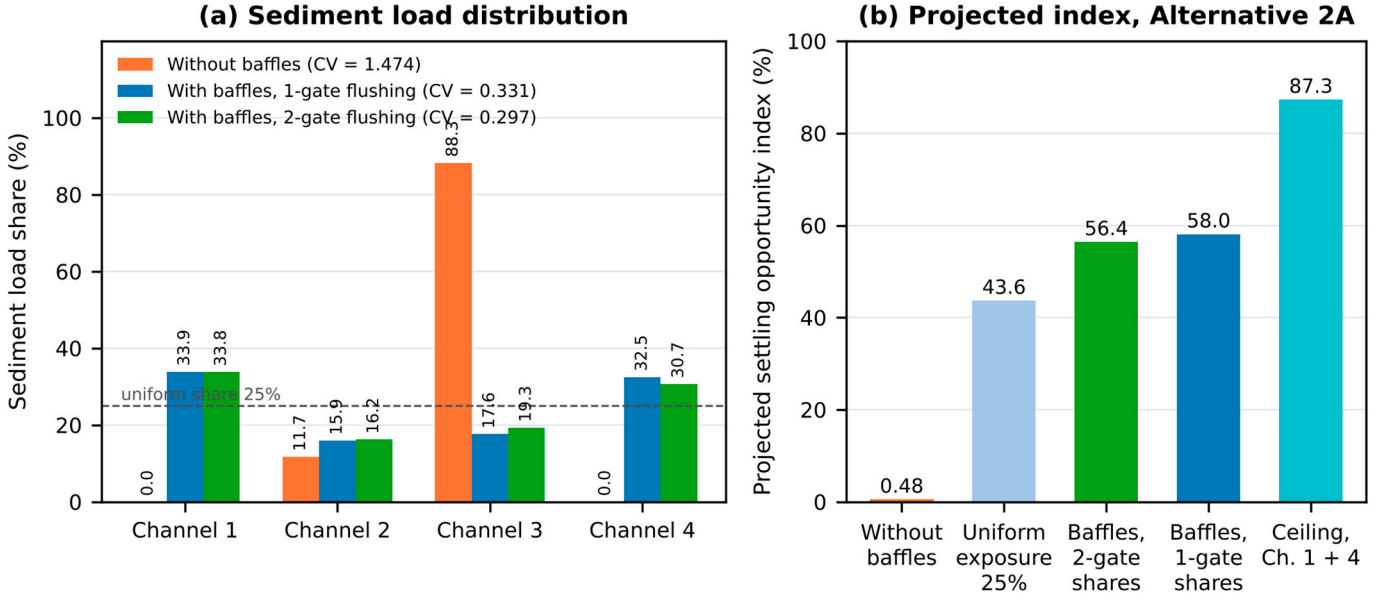


Figure 8. Simulated effect of installing baffles in Alternative 2A: (**a**) sediment load distribution without and with baffles under simulated flushing condition; (**b**) exploratory projection of settling opportunity index based on alternative channel-load distributions.

Table 10. Mass balance and time performance of two flushing scenarios (discharge 7.5 m^3/s).

Quantity	1-Gate Flushing	2-Gate Flushing (Full Opening)	Difference
Simulation duration	683.0 s	679.0 s	—
Flushed sediment mass	246.2 t	248.4 t	+0.9%
Water volume used	13,260 m^3	12,538 m^3	−5.4%
Water per kilogram of sediment	0.0539 m^3/kg	0.0505 m^3/kg	−6.3%
Mean discharge	19.36 m^3/s	18.42 m^3/s	−4.9%
Mean concentration	18.54 kg/m^3	19.80 kg/m^3	+6.8%
Onset of sediment transport	71.0 s	110.0 s	39 s later
Time to peak	96.0 s	178.0 s	—
Peak rate	2.012 kg/s	1.343 kg/s	−33%
Time to half of the mass (T_{50})	178.0 s	234.0 s	—
Time to nine-tenths of the mass (T_{90})	342.0 s	428.0 s	—
Maximum bed lowering	0.117 m	0.117 m	equal

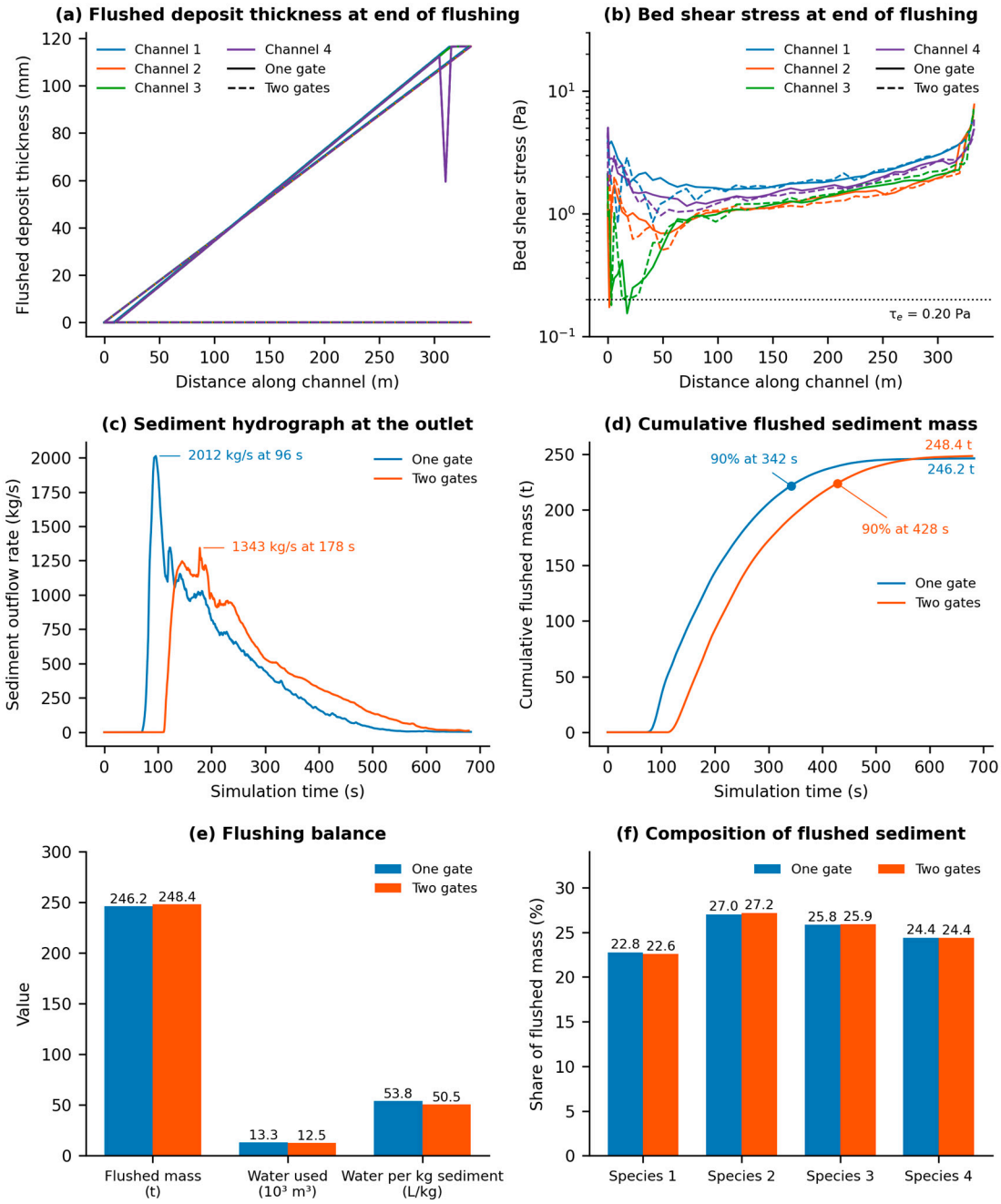


Figure 9. Flushing analysis on real-time basis for one-gate and two-gate scenarios: deposit thickness, bed shear stress, sediment hydrograph, cumulative flushed mass, flushing balance, and grain-size sorting.

3.6. Validation of Numerical Model Against Physical Model

The FLOW-3D model reproduced the physical model water levels very well and the flow velocities well (Table 11; Figure 10). The numerical water surface tended to be slightly more uniform than in the physical model, which varied more between cross-sections. Because chambers A and D had reverse flow (signed velocities ±), the magnitude-based PBIAS (+8.59%) was more representative than the signed PBIAS (−11.26%).

Table 11. Validation statistics of FLOW-3D Hydro against 1:5 physical model (Q50%, Q100%, and Q120%).

Parameter	Number of Points	Relative MAE (%)	RMSE	PBIAS (%)
Water level	69	6.43	0.024 m	−4.73 (slight overestimate)
Flow velocity	23	12.50	0.044 m/s	+8.59 (magnitude); −11.26 (signed)

Notes: PBIAS = Σ(measured − simulated)/Σ measured × 100; positive values indicate underestimation by the numerical model and negative values overestimation.

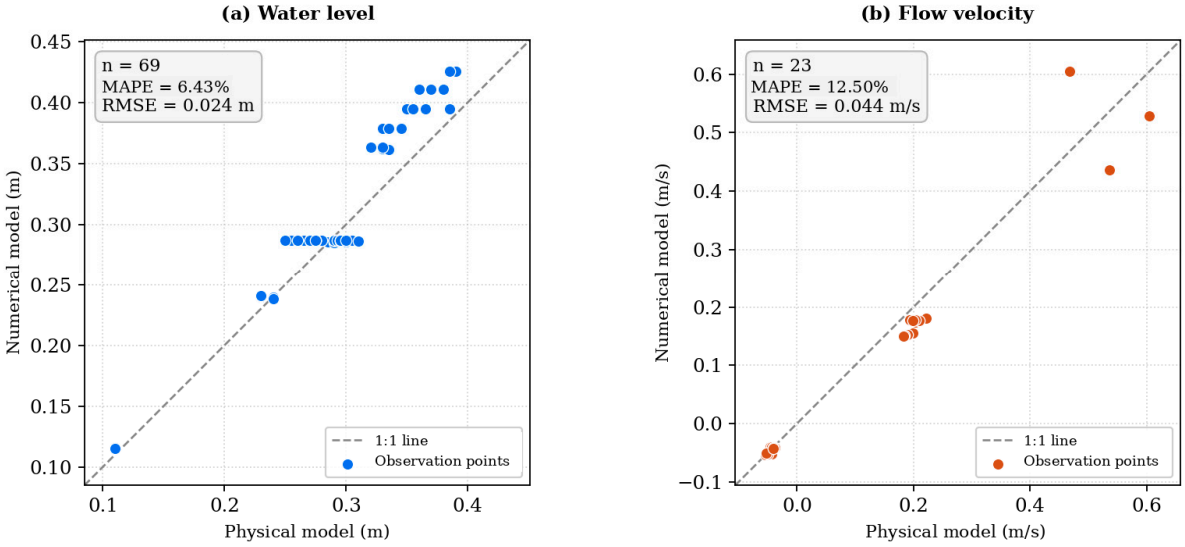


Figure 10. Validation of numerical model against physical model (1:1 line = ideal): (**a**) water level; (**b**) flow velocity.

4. Discussion

The sediment samples collected at Warujayeng IA indicated that the material found downstream of the sediment excluder was predominantly fine-grained, comprising 74.59–75.01% silt and 20.97–21.79% clay. However, because the assessment was based on only two downstream samples, and no corresponding upstream samples were collected, these data do not permit a quantitative estimation of sediment-exclusion efficiency or establish that the structure retained no fine sediment. The findings should therefore be interpreted as evidence of the fine-grained sediment present downstream, rather than as a direct measurement of the structure's retention performance. At Koya Tami IA, the sampled sediment contained cohesive fractions of 77–100%. The HEC-RAS 2D simulation indicates that the existing Tami Weir sand trap reduced velocities to below 0.1 m/s and estimates a trapping efficiency of approximately 27% under the adopted model parameters. This finding is consistent with Theol [23] and with recent studies of flocculation and erosion thresholds [20–22], showing that cohesive sediment behaves differently from non-cohesive sediment and is difficult both to settle and to flush, and it extends the split and settle studies [25,26], which were limited to fine non-cohesive sand. This model-based estimate is comparable to the 27% trapping efficiency of the Lower Usuthu sand trap before modification [26], although the sediment at that site is much coarser.

The HEC-RAS estimate of sediment trapping at Tami Weir is subject to uncertainty associated with the selected cohesive-sediment parameters. Although the critical erosion shear stress was set to T_c = 0.20 N/m^2 based on the reported range for moderately consolidated silt, no systematic sensitivity analysis was conducted for the Partheniades erodibility

coefficient, the critical erosion threshold, or the Krone deposition parameters. The influence of these parameters on predicted erosion, deposition, and trapping efficiency therefore remains unquantified. Accordingly, the estimated trapping efficiency of approximately 27% should be interpreted as a model-based result under the adopted parameter settings, rather than as a field-validated measure of sediment retention. Future work should evaluate parameter sensitivity and calibrate the cohesive-sediment formulation against site-specific measurements of erosion resistance, deposition, and sediment mass balance.

A key constraint on the settling opportunity in both alternatives is the high surface loading rate. The simulated rates of 2.19–8.14 m/h exceed the 0.5–1.5 m/h reference range for fine sediment, while the minimum settling velocity required for particles to reach the bed before leaving the structure is 0.61–2.26 mm/s, compared with approximately 0.13 mm/s for the reported 12 µm field grains. Because the simulations used 0.03–0.0625 mm sediment classes, their settling behaviour does not directly represent that of the finer field material. The resulting settling estimates should therefore be interpreted as conditional on the specified particle sizes and hydraulic conditions. Increasing the settling path or reducing the unit discharge warrants investigation as a means of improving settling opportunity. Flocculation should not be assumed to compensate for the high surface loading rate. Although the simulated concentrations of 81–142 mg/L are below the 599–1530 mg/L range identified for significant flocculation under the applied correction, freshwater floc formation can also depend on turbulent shear and mineralogy [20], while extracellular polymeric substances may influence floc settling behaviour [21]. The effective settling velocity of sediment from the Tami River should therefore be measured directly, for example, through settling-column tests, before the contribution of flocculation is ruled out.

The comparison of Alternatives 2A and 2B indicates a trade-off between sediment load distribution and the availability of low-shear channels. Alternative 2B had the most uniform simulated load distribution (coefficient of variation, 0.211), but no channel provided sufficiently favourable settling conditions under the adopted criterion, resulting in a maximum settling opportunity index of only 0.08%. Alternative 2A had two channels with more favourable low-shear conditions (reported ceiling of 87.26%), but its inlet load distribution was uneven. The baffled simulations indicate that inlet baffles can improve the distribution of simulated sediment load among the channels under the tested flushing condition. This finding identifies a design option for further investigation while retaining the four-channel arrangement; it does not, by itself, demonstrate improved cohesive-sediment trapping. The influence of inlet baffles on flow distribution is consistent with findings from settling-tank simulations [37], while the role of flow-splitting structures in controlling discharge and sediment concentration distribution has also been reported for the split-and-settle trap [20]. Applying the simulated channel-load shares obtained at a flushing discharge of 7.5 m^3/s to the channel-specific settling opportunity indices calculated at a settling discharge of 5.0 m^3/s yields an exploratory projected system index of 56.37–58.04%. Because this estimate combines results from different discharge conditions and because the baffles may alter the flow field and bed shear stress at 5.0 m^3/s, it should be treated as an exploratory upper-bound estimate rather than a validated performance measure or trapping efficiency. A dedicated simulation of the baffled configuration at a settling discharge of 5.0 m^3/s is required to assess its settling opportunity under consistent hydraulic conditions.

The flushing simulations indicate that 90% of the sediment mass mobilised during the numerical runs was transported by 342 s under one-gate opening and by 428 s under full-gate opening. These results suggest that approximately seven minutes is sufficient to remove most of the sediment that is readily mobilised under the simulated conditions; however, this duration should not be interpreted as an established operational requirement for cohesive-sediment deposits. FLOW-3D Hydro uses a non-cohesive sediment formulation

and does not explicitly represent cohesive flocculation or the increase in erosion resistance associated with deposit consolidation. The simulated flushing duration therefore requires verification through physical sediment-transport tests and field monitoring before it can be recommended for operational use. The comparison between gate configurations also warrants caution: full-gate opening removed 248.4 t, compared with 246.2 t under one-gate opening, a difference of only 0.9%. Although full-gate opening used 6.3% less water per kilogram of sediment removed in the simulations, no uncertainty analysis was conducted to establish whether this difference is robust. Full-gate opening may therefore be considered a candidate operating scenario based on simulated water-use efficiency, rather than a definitive recommendation for superior sediment removal. Previous physical model studies of flushing at run-of-river hydropower plants have examined flushing efficiency under different conditions [38], while HEC-RAS-based protocols in the Progo-Opak-Serang basin recommend flushing durations of 45–150 min three to four times a year [6]. These comparisons provide operational context but do not establish an appropriate duration for the present structure or its cohesive deposits. The duration and gate-opening strategy should be determined through further physical model testing and field monitoring, consistent with the importance of operating procedures in sediment management [17,18].

The series 0 validation evaluated the hydraulic representation of FLOW-3D by comparing simulated water levels and velocities with the physical model, yielding relative MAEs of 6.43% and 12.50%, respectively. This agreement supports the use of the model for analysing the flow field within the tested hydraulic conditions, but it does not validate sediment transport or cohesive-sediment deposition. The FLOW-3D sediment formulation used here is non-cohesive and applies a single Shields-based criterion, whereas the cohesive-sediment interpretation relies on literature-derived deposition and erosion thresholds. Consequently, the model does not explicitly reproduce the transition between deposition below the selected cohesive-sediment threshold and erosion above the selected erosion threshold, nor does it resolve cohesive flocculation or consolidation-dependent erosion resistance. The settling opportunity index is therefore a threshold-based diagnostic derived from the simulated bed shear-stress field, not a validated measure of cohesive-sediment trapping efficiency.

The role of bed evolution also requires consideration when interpreting the simulated sediment transport results. Deposition changes the local bed elevation and flow depth, while erosion can expose a different bed configuration; both processes may alter the local velocity distribution and bed shear stress. These changes can, in turn, affect whether subsequent sediment is deposited or remobilised relative to the selected critical shear-stress thresholds. The present analysis does not independently quantify or validate this feedback under field-scale cohesive-sediment conditions. Consequently, the settling opportunity indices and flushing results should be interpreted as conditional on the simulated hydraulic and sediment conditions, rather than as predictions that account fully for the evolving behaviour of cohesive deposits. Future physical sediment-transport tests and field monitoring should document changes in bed elevation alongside flow and sediment measurements to evaluate this feedback.

Validation of the sediment aspects is proposed to cover three quantities: (1) load distribution among channels (27.6:32.4:20.1:19.9% in Alternative 2B, 0.0:11.7:88.3:0.0% in Alternative 2A without baffles, and about 34:16:18:32% in the baffled model), (2) the location of the deposition centroid, namely, 27–34 m for half of the mass and 82–109 m for nine-tenths of the mass, equivalent to 5.4–6.8 m and 16.4–21.8 m in the model, so the 60 m flume covers the entire working zone, and (3) flushing performance, namely, nine-tenths of the mass flushed within 342–428 s in the prototype or 153–191 s in the model. The 1:5 test parameters can be set directly from the simulation results: settling discharge 89.44 L/s,

flushing discharge 134.16 L/s, flushing duration 305 s, flushing velocity 0.67 m/s, erosion threshold 0.04 N/m^2, and deposition threshold 0.012 N/m^2.

These findings may inform the future evaluation of design criteria for cohesive-sediment traps in KP-04, but they should not yet be treated as validated design requirements. Candidate parameters for further investigation include a surface loading rate within the 0.5–1.5 m/h reference range, bed shear stress below a sediment-specific deposition threshold along the settling path, more uniform sediment-load distribution among channels, and an appropriate flushing duration and gate-opening pattern. The applicable limits will require further assessment using site-specific sediment properties, numerical simulations at the settling discharge, and physical sediment transport tests. Upstream sediment-reduction measures, such as river normalisation, groundsills, and check dams to control riverbed change and woody debris, may also support sediment management, although their effects were not quantitatively analysed in this study. Vulnerability mapping of sand traps in tropical volcanic watersheds indicates that structures at the outlets of sub-watersheds with high sediment yields are particularly vulnerable, whereas dense forest cover is associated with lower vulnerability [5]. A similar assessment could be considered for the Tami watershed in view of the reported upstream land-cover changes. The main limitations of this study include the absence of upstream sediment samples at Warujayeng IA, the non-cohesive sediment formulation used in FLOW-3D Hydro, and the ongoing physical model sediment-transport tests.

5. Conclusions

The KP-02 and KP-04 criteria provide limited guidance for cohesive sediment. At Warujayeng IA, the two downstream samples contained 74.59–75.01% silt and 20.97–21.79% clay; because no upstream samples were collected, these data do not quantify the sediment excluder's efficiency. At Tami Weir, HEC-RAS 2D estimated a trapping efficiency of approximately 27% for sediment with cohesive fractions of 77–100%, under the adopted model parameters. FLOW-3D Hydro simulations, validated hydraulically against a 1:5 physical model (relative MAEs of 6.43% for water level and 12.50% for velocity), indicate that settling opportunity is influenced by bed shear stress and sediment load distribution among channels. Without baffles, the settling opportunity indices were 0.48% for Alternative 2A and 0.02% for Alternative 2B, while surface loading rates of 2.19–8.14 m/h exceeded the 0.5–1.5 m/h reference range.

Alternative 2A with inlet baffles is proposed as a reference configuration for further silt settler development because the baffles reduce the coefficient of variation of channel-load distribution from 1.474 to 0.297–0.331 under the simulated flushing condition. The projected settling opportunity index of 56.4–58.0% is an exploratory upper-bound estimate based on channel-load shares at 7.5 m^3/s and channel-specific settling opportunity indices at 5.0 m^3/s; it is not a validated trapping efficiency. The actual settling performance of the baffled configuration remains to be established through additional numerical simulations at the settling discharge and subsequent physical model sediment-transport tests. The surface loading rate also needs to be reduced by lengthening the settling path or reducing the unit discharge. Full-gate-opening flushing at 7.5 m^3/s is proposed for further evaluation, with a simulated duration of about seven minutes for the readily mobilised deposits. Further research should (1) simulate the baffled configuration at the settling discharge of 5.0 m^3/s, (2) complete the sediment-transport tests in the physical model using the planned Rouse number scaling (model diameter 0.050 mm), (3) evaluate the Warujayeng IA sediment excluder with simultaneous upstream and downstream sampling, and (4) integrate biological processes and mixed sediment. The proposed configuration may

inform the future development of a silt settler prototype and potential revisions to KP-04, subject to further validation.

Author Contributions: Conceptualisation, H.K.K.; methodology, H.K.K. and W.A.P.; investigation, H.K.K.; formal analysis, H.K.K.; validation, H.K.K. and W.A.P.; writing—original draft preparation, H.K.K.; writing—review and editing, H.K.K., A.P.I. and W.A.P.; supervision, A.P.I. and W.A.P. All authors have read and agreed to the published version of the manuscript.

Funding: This research received no external funding.

Data Availability Statement: The original contributions presented in this study are included in the article. Further inquiries can be directed to the corresponding author.

Acknowledgments: The authors thank the Water Resources Engineering Laboratory and the Irrigation and Hydraulic Structures Laboratory, Institut Teknologi Bandung (ITB), Jatinangor Campus, for the physical model testing facilities; the Head of the Papua River Basin Organization (BWS Papua) for permission to use Tami Weir as a study site; F.X. Suryadi (IHE Delft Institute for Water Education) and Slamet Imam Wahyudi (UNISSULA Semarang) for their input; PT Aditya Engineering Consultant and PT Bima Sakti Geotama; and Andhika Wicaksono and Dazztech Solutions Sdn Bhd (FLOW-3D) for their support.

Conflicts of Interest: The authors declare no conflicts of interest.

Abbreviations

The following abbreviations are used in this manuscript:

ADV	Acoustic Doppler Velocimeter
CFD	Computational Fluid Dynamics
IA	Irrigation Area (Daerah Irigasi)
HEC-RAS	Hydrologic Engineering Center's River Analysis System
KP	Kriteria Perencanaan Irigasi (Indonesian Irrigation Design Criteria)
MAE	Mean Absolute Error
O&M	Operation and Maintenance
PBIAS	Percent Bias
RANS	Reynolds-Averaged Navier–Stokes
RMSE	Root Mean Square Error
RNG	Renormalisation Group
TSS	Total Suspended Solids
VOF	Volume of Fluid

References

1. Kementerian Pekerjaan Umum dan Perumahan Rakyat; Direktorat Jenderal Sumber Daya Air. *Surat Edaran Nomor 01/SE/D/2019 Tentang Pedoman Teknis Modernisasi Irigasi*; Kementerian Pekerjaan Umum dan Perumahan Rakyat; Direktorat Jenderal Sumber Daya Air: Jakarta, Indonesia, 2019.
2. Zayed, M.; Abdelmoaty, M.S. Assessing the Morphological Changes on the Operation Performance of Canal: A Case Study of the Suez Irrigation Canal, Egypt. *Water Pract. Technol.* **2024**, *19*, 36–51. [CrossRef]
3. Gabr, M.E.; Fattouh, E.M.; Mostafa, M.K. Determination of the Canal Discharge Capacity Ratio and Roughness to Assess Its Maintenance Status: Application in Egypt. *Water* **2023**, *15*, 2387. [CrossRef]
4. Tirtalistyani, R.; Murtiningrum, M.; Kanwar, R.S. Indonesia Rice Irrigation System: Time for Innovation. *Sustainability* **2022**, *14*, 12477. [CrossRef]
5. Pradipta, A.G.; Loc, H.H.; Park, E.; Prihanantya, A.S.; Nurhady, S.; Setyawan, C.; Mohanasundaram, S.; Virdis, S.G.P.; Shrestha, S. Mapping the Vulnerability of Irrigation Sand Traps in a Tropical Volcanic Basin, Indonesia. *Sci. Rep.* **2023**, *13*, 18188. [CrossRef] [PubMed]
6. Pradipta, A.G.; Loc, H.H.; Nurhady, S.; Murtinigrum; Arif, S.S. Managing Irrigation Sediment Barriers in a Tropical Volcanic Basin through Mathematical Model. *ACS ES&T Water* **2024**, *4*, 3798–3815. [CrossRef]
7. Kementerian Pekerjaan Umum. *Standar Perencanaan Irigasi: Kriteria Perencanaan Bagian Bangunan Utama (KP-02) Dan Bagian Bangunan (KP-04)*; Kementerian Pekerjaan Umum: Jakarta, Indonesia, 2013.
8. Atkinson, E. Vortex-Tube Sediment Extractors. I: Trapping Efficiency. *J. Hydraul. Eng.* **1994**, *120*, 1110–1125. [CrossRef]

9. Kothyari, U.C.; Pande, P.K.; Gahlot, A.K. Design for Tunnel-Type Sediment Excluder. *J. Irrig. Drain. Eng.* **1994**, *120*, 36–47. [CrossRef]
10. Sharafati, A.; Haghbin, M.; Tiwari, N.K.; Bhagat, S.K.; Al-Ansari, N.; Chau, K.-W.; Yaseen, Z.M. Performance Evaluation of Sediment Ejector Efficiency Using Hybrid Neuro-Fuzzy Models. *Eng. Appl. Comput. Fluid Mech.* **2021**, *15*, 627–643. [CrossRef]
11. Nan, J.; Du, S.; Hu, H.; Xu, C.; Li, W. Numerical Simulation of Water–Sediment Characteristics in a Trapezoidal Desilting Channel with a Swirling Flow Generator. *J. Irrig. Drain. Eng.* **2025**, *151*, 04025016. [CrossRef]
12. Nie, L.; Jin, J.; Ma, Y.; Li, X.; Wang, Z. Factors Affecting Sediment Deposition Thickness in Irrigation Channels and the Impact of Deposition on Stage–Discharge Measurement. *Appl. Sci.* **2025**, *16*, 121. [CrossRef]
13. Paudel, K. Role of Sediment in the Design and Management of Irrigation Canals: Sunsari Morang Irrigation Scheme, Nepal. Ph.D. Thesis, Wageningen University, Wageningen, The Netherlands, 2010.
14. Sutama, N.H. *Mathematical Modelling of Sediment Transport and Its Improvement in Bekasi Irrigation System, West Java, Indonesia*; UNESCO-IHE Institute for Water Education: Delft, The Netherlands, 2010.
15. Hu, J. Study on Mathematical Modeling for Non-Uniform Sediment Transport in an Irrigation District along the Lower Reach of the Yellow River. *J. China Inst. Water Resour. Hydropower Res.* **2008**, *1*, 005.
16. Munir, S. Role of Sediment Transport in Operation and Maintenance of Supply and Demand Based Irrigation Channels: Application to Machai Maira Branch Canals. Ph.D. Thesis, Wageningen University, Wageningen, The Netherlands, 2011.
17. Osman, I.S.E. Impact of Improved Operation and Maintenance on Cohesive Sediment Transport in Gezira Scheme, Sudan. Ph.D. Thesis, Wageningen University, Wageningen, The Netherlands, 2015.
18. Theol, S.A.; Jagers, B.; Suryadi, F.X.; de Fraiture, C. The Role of Gate Operation in Reducing Problems with Cohesive and Non-Cohesive Sediments in Irrigation Canals. *Water* **2019**, *11*, 2572. [CrossRef]
19. Krishnappan, B. Review of a Semi-Empirical Modelling Approach for Cohesive Sediment Transport in River Systems. *Water* **2022**, *14*, 256. [CrossRef]
20. Theol, S.A.A.A. The Use of Delft3D to Simulate the Deposition of Cohesive and Non-Cohesive Sediments in Irrigation Systems. Ph.D. Thesis, Wageningen University, Leiden, The Netherlands, 2020.
21. Chao, X.; Hossain, A.K.M.A.; Al-Hamdan, M.Z.; Jia, Y.; Cizdziel, J.V. Three-Dimensional Numerical Modeling of Flow Hydrodynamics and Cohesive Sediment Transport in Enid Lake, Mississippi. *Geosciences* **2022**, *12*, 160. [CrossRef]
22. Nghiem, J.A.; Fischer, W.W.; Li, G.K.; Lamb, M.P. A Mechanistic Model for Mud Flocculation in Freshwater Rivers. *J. Geophys. Res. Earth Surf.* **2022**, *127*, e2021JF006392. [CrossRef]
23. Mc Leod, C.; Bosman, A.; Smit, F. Numerical and Field Investigation to Improve an Existing Distributed-Sediment-Excluder Sand Trap Performance. *AQUA—Water Infrastruct. Ecosyst. Soc.* **2025**, *74*, 199–219. [CrossRef]
24. McLeod, C.; Bosman, A.; Smit, F. Hydrodynamics and Sediment Concentration Distribution in a Split-and-Settle Sand Trap: A Physical and Numerical Model Investigation. *J. Hydroinform.* **2025**, *27*, 1102–1120. [CrossRef]
25. Sawadogo, O. Coupled Fully Three-Dimensional Mathematical Modelling of Sediment Deposition and Erosion in Reservoirs. Ph.D. Thesis, Stellenbosch University, Stellenbosch, South Africa, 2015.
26. Wongtragoon, U.; Kubo, N.; Tanji, H. A Study on Improving Sand Trap in a Large Scale of Irrigation Scheme. In *2nd World Irrigation Forum (WIF2)*; International Commission on Irrigation and Drainage (ICID): New Delhi, India, 2016; pp. 1–13.
27. Pradipta, A.G.; Loc, H.H.; Nurhady, S.; Murtiningrum; Mohanasundaram, S.; Park, E.; Shrestha, S.; Arif, S.S. Mathematical Modeling-Based Management of a Sand Trap throughout Operational and Maintenance Periods (Case Study: Pengasih Irrigation Network, Indonesia). *Water* **2022**, *14*, 3081. [CrossRef]
28. Ye, L.; Penaloza-Giraldo, J.A.; Manning, A.J.; Holyoke, J.; Hsu, T.-J. Biophysical Flocculation Reduces Variability of Cohesive Sediment Settling Velocity. *Commun. Earth Environ.* **2023**, *4*, 138. [CrossRef]
29. Chen, D.; Zheng, J.; Zhang, C.; Guan, D.; Li, Y.; Wang, Y. Critical Shear Stress for Erosion of Sand-Mud Mixtures and Pure Mud. *Front. Mar. Sci.* **2021**, *8*, 713039. [CrossRef]
30. Hydrologic Engineering Center. *HEC-RAS 2D Sediment User Manual*; Hydrologic Engineering Center: Davis, CA, USA, 2024.
31. Pratama, F.; Wulandari, S.; Rohmat, F.I.W. Modeling Sediment Accumulation in Pare Reservoir Using HEC-RAS 2D: Assessing Storage Capacity over a 10-Year Period. *Results Eng.* **2025**, *25*, 104333. [CrossRef]
32. Partheniades, E. Erosion and Deposition of Cohesive Soils. *J. Hydraul. Div.* **1965**, *91*, 105–139. [CrossRef]
33. Krone, R.B. *Flume Studies of the Transport of Sediment in Estuarial Shoaling Processes: Final Report*; Hydraulic Engineering Laboratory and Sanitary Engineering Research Laboratory, University of California: Berkeley, CA, USA, 1962.
34. Zandonadi Moura, L.; Martinez, J.-M.; Santini, W.; Koide, S.; Llacer Roig, H.; Alves e Santos, D.R.; Soares, A.K. Sediment Transport Modeling for Run-of-River Hydropower in the Madeira River: Calibration with Conventional and Remote Sensing Data. *Int. J. Sediment Res.* **2025**, *40*, 777–790. [CrossRef]
35. Zaffar, M.W.; Haasan, I.; Ghumman, A.R. Performance Evaluation of Different Stilling Basins Downstream of Barrage Using FLOW-3D Scour Models. *Hydrology* **2023**, *10*, 223. [CrossRef]

36. van Leussen, W. Estuarine Macroflocs and Their Role in Fine-Grained Sediment Transport, Utrecht University, Utrecht, The Netherlands, 1994.
37. Bruno, P.; Bruno, F.; Di Bella, G.; Napoli, E.; De Marchis, M. CFD Study on the Effect of the Baffles Geometry in Sedimentation Efficiency in Wastewater Treatments through Large Eddy Simulations. *J. Environ. Manag.* **2025**, *373*, 123536. [CrossRef] [PubMed]
38. Gold, T.; Reiterer, K.; Hauer, C.; Habersack, H.; Sindelar, C. Flushing Efficiency of Run-of-River Hydropower Plants: Novel Approaches Based on Physical Laboratory Experiments. *Water* **2023**, *15*, 2657. [CrossRef]

Disclaimer/Publisher's Note: The statements, opinions and data contained in all publications are solely those of the individual author(s) and contributor(s) and not of MDPI and/or the editor(s). MDPI and/or the editor(s) disclaim responsibility for any injury to people or property resulting from any ideas, methods, instructions or products referred to in the content.